



Available online at www.sciencedirect.com

ScienceDirect

Procedia Structural Integrity 68 (2025) 506-512



European Conference on Fracture 2024

The microstructure and fracture mode of physically simulated heataffected zones of a weld metal used with 500 MPa offshore steel – part 2: fractographies, inclusions and microstructures

Henri Tervo^{a,*}, Marcell Gáspár^b, Judit Kovács^b, Antti Kaijalainen^a, Vahid Javaheri^a, Johannes Sainio^c, Jukka Kömi^a

^aMaterials and Mechanical Engineering, Centre for Advanced Steel Research, University of Oulu, P.O. Box 4200, Oulu, FI-90014, Finland ^bInstitute of Material Science and Technology, University of Miskolc, Miskolc-Egyetemváros, HU-3515, Hungary ^cSSAB Europe, Rautaruukintie 155, P.O. Box 93, Raahe, FI-92101, Finland

Abstract

Welded joints in 500 MPa offshore steels are often the weakest points in structures, and multiple welding passes for thick sections can affect the microstructure of the weld metal. While much research focuses on heat-affected zones (HAZ) in the base metal, this study examines the HAZ in the weld metal, comparing the original weld's microstructure, inclusions, and fracture modes to simulated coarse-grained (CGHAZ-W) and intercritical HAZs (ICHAZ-W) in the weld metal. The original weld was produced using submerged arc welding, and HAZs with different cooling times ($t_{8/5} = 5$, 15, 30 s) were simulated using a Gleeble 3500 thermomechanical simulator. Microstructural analysis, inclusion measurements, and fractography were performed using a field emission scanning electron microscope. The results showed that thermal cycles altered the microstructure of CGHAZ-W and ICHAZ-W compared to the original weld. The shortest cooling time ($t_{8/5} = 5$ s) led to slight hardening in CGHAZ-W. Inclusions, mainly oxides or oxysulfides, increased significantly in CGHAZ-W, but not in ICHAZ-W. Most samples exhibited ductile fractures, with microvoid nucleation, although local brittle regions were detected, linked to grain boundary ferrite and side-plate ferrite in an acicular ferritic matrix.

© 2025 The Authors. Published by ELSEVIER B.V.
This is an open access article under the CC BY-NC-ND license (https://creativecommons.org/licenses/by-nc-nd/4.0)
Peer-review under responsibility of ECF24 organizers

Keywords: steel; welding; microstructure; inclusions; Gleeble; HAZ; fractography

* Corresponding author. Tel.: +358442761001 *E-mail address*: henri.tervo@oulu.fi

1. Introduction

High strength offshore steels are developed for demanding conditions where both high strength and toughness are required from the materials to ensure the integrity and safe performance of structures made from them. Some of the typical applications for such steels are offshore oil drilling platforms, wind power mills and ships. For example, some parts of Valhall oil drilling platform in Norway were constructed using 500 MPa offshore steels (Willms, 2009).

As a result of thermomechanically controlled hot rolling process, the microstructure of 500 MPa offshore usually consists of fine-grained bainite and ferrite. However, the original microstructure is altered when steels are welded. The thermal cycles originating from the welding process cause different type of heat-affected zones (HAZ) depending on the peak temperature and cooling rate of each location in the steel. Additionally, welding of thick steel sections may require multiple passes causing additional thermal cycles on already altered microstructure as well as on the weld metal produced during previous passes.

The most important HAZs where the properties are expected to change are coarse-grained (CGHAZ), intercritical (ICHAZ) and intercritically reheated coarse-grained HAZ (ICCGHAZ). Each of these zones is usually relatively narrow making it challenging to precisely characterize their microstructures and mechanical properties.

Physical simulation provides a way to produce microstructures imitating those of the different type of HAZs on sufficiently large area for mechanical tests and microstructural examination. It also makes possible to study the effect of different welding methods and parameters by adjusting simulation parameters. Consequently, physical simulation is nowadays rather common way to study the HAZ microstructures and properties (Mičian et al., 2020; Węglowski et al., 2013). However, there are less studies where the physical simulation has been applied on studying HAZs on weld metal caused by subsequent welding passes (Kang et al., 2018; Tezuka et al., 1995). Therefore, the aim of this study was to evaluate the effect of multipass welding on the weld metal by examining its microstructure, inclusion content and fractured Charpy V-notch impact toughness testing samples after physical simulation of HAZ.

2. Materials and methods

The studied base material is a 16 mm thick 500 MPa offshore steel that was welded by single-pass submerged arc welding (SAW) method. The filler material is ESAB OK 13.24, a Ni- and Mo-alloyed, Cu-coated wire for SAW. The flux used with the filler material is OK Flux 10.62. The chemical compositions as well as the A_{c1} and A_{c3} temperatures (calculated by JMatPro v12.2) of the base material and the filler material are presented in Table 1. The following welding settings were applied: the root gap 3 mm, the edge width 4 mm and the bevel angle 40°.

	С	Si	Mn	P	S	Cu	Cr	Mo	Ni	A_{c1}	A _{c3}
Base	≤0.14	≤0.6	≤1.7	≤0.02	≤0.01	≤0.55	Cr+Mo	≤0.65	≤2.00	626	847
Filler	0.07	0.18	1.3	0.015	0.008	0.06	0.05	0.2	0.78	672	826

Table 1. Chemical composition (wt.%), and Ac1 and Ac3 temperatures (°C) of the studied base metal and filler metal.

 $70 \times 10 \times 10 \text{ mm}^3$ specimens were machined keeping the welded joint in the middle. These specimens were used for the HAZ-W simulations. Example of the specimen is shown in the part 1 of the study (Gáspár et al., 2024).

Thermomechanical simulator Gleeble 3500 was used to produce coarse-grained (CGHAZ-W) and intercritical (ICHAZ-W) HAZ on the weld metal. Each of the HAZ was simulated using three different cooling time from 800 °C to 500 °C ($t_{8/5} = 5$, 15 and 30 s) to represent the typical welding parameter variation. Peak temperature of CGHAZ-W simulations was 1350 °C, whereas in ICHAZ-W simulations it was 815 °C defined by determining the A_{c1} temperature of the steel by using a dummy sample and adding 50 °C to it. Simulation was based on Rykalin-3D model.

Microstructure of the simulated HAZ-Ws was studied using field emission scanning electron microscope (FESEM, Zeiss Sigma). The acceleration voltage was 5 kV and the working distance varied approximately between 4 and 6 mm. The samples for microstructural characterization were cut from the Gleeble specimens keeping the simulation region in the middle. The samples were placed in specimen holders, grinded, polished and Nital-etched before the FESEM examination.

Charpy V-notch (CVN) impact toughness testing was performed using PSD 300 instrumented impact toughness tester for the simulated HAZ samples. The sample size was $50 \times 10 \times 10$ mm³ and the testing temperature was -40 °C. The CVN results are presented and discussed fully in the first part of the study published simultaneously in a separate paper (Gáspár et al., 2024).

Fractographies of the tested CVN samples were studied using a JEOL JSM 7900F field emission scanning electron microscope (FESEM). The acceleration voltage was 5 kV and the working distance approximately 8–11 mm.

Non-metallic inclusions in the weld metals were studied using JEOL JSM 7900F FESEM together with energy dispersive spectroscope (EDS). Inclusions were scanned from a predefined area of polished cross-section samples using the acceleration voltage of 15 kV and the working distance of approximately 10 mm. The scanned area varied in the range of 3.6–10.8 mm² and the minimum inclusion length taking into account was 1 µm. For acquiring and analyzing the data, Oxford's AZTEC software was used.

Inclusions were classified using a Karakterizer tool (Tervo et al., 2023), which is based on the classification method developed at the University of Oulu and published in 2018 (Alatarvas, 2018).

3. Results and discussion

3.1. Microstructures

The simulated HAZ-Ws as well as the original weld metal were examined by the FESEM. The original single-pass weld metal consisted of acicular ferrite (AF). AF is a type of intergranular ferrite nucleating on certain type of non-metallic inclusions inside the prior austenite grains. AF consists of chaotically oriented needle-like grains with the width and length of approximately $1-3~\mu m$ and $5-15~\mu m$, respectively. These grains form a complex interlocking structure, which efficiently prevents the crack propagation, enhancing the fracture toughness properties of the steel (Loder et al., 2016; Xiong et al., 2015). Beside AF, grain boundary ferrite and ferrite side-plates were observed near the prior austenite grain boundaries. These types of microstructures are coarser than AF and may be more susceptible to brittle fracture. The original weld metal microstructure of the studied steel with the measured hardness as a reference is presented in Fig. 1a.

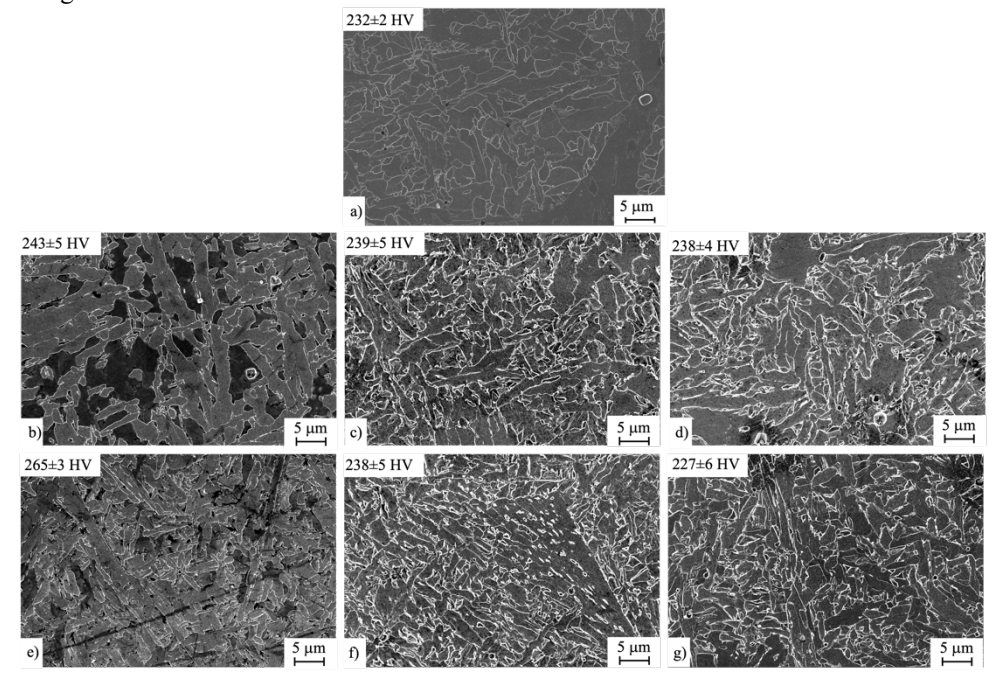


Fig. 1. FESEM images of the original weld (a) as well as simulated ICHAZ-W (a, b, c) and CGHAZ-W (d, e, f) using the $t_{8/5} = 5$ s, 15 s, and 30 s, respectively.

Intercritical HAZ of the weld (ICHAZ-W) was simulated using the peak temperature 815 °C. The steel is partly austenitized in this temperature, resulting in some changes in the microstructure. The applied cooling times from 800 °C to 500 °C ($t_{8/5}$) were 5 s, 15 s, and 30 s to simulate the practical heat input range of the SAW process. Fig. 1 (b, c, d) show the ICHAZ-W microstructures with the $t_{8/5} = 5$ s, 15 s, and 30 s, respectively.

The peak temperature for the coarse-grained HAZ of the weld (CGHAZ-W) simulation was 1350 °C. Therefore, the steel was fully austenitized since the simulation temperature is above A_{c3} temperature of the weld metal as seen in Table 1. In this case, it is expected that the prior austenite grain growth occurs. The transformation microstructure depends on the cooling rate. Using high heat input, the cooling rate slows down (cooling time increases), and the resulting microstructure is less hardened than with low heat input welding. The CGHAZ-W microstructures with the $t_{8/5} = 5$ s, 15 s, and 30 s are presented in Fig. 1 (e, f, g), respectively.

CGHAZ-W with $t_{8/5} = 5$ s exhibited a slight hardening, with the measured HV_{10} hardness increasing by about 30 HV compared to the original weld metal. In other studied variants the hardness remained approximately in the level of the original weld metal. The hardening in CGHAZ-W with $t_{8/5} = 5$ s might be attributed to the finer grains of acciular ferrite (AF), but also bainite transformation may have occurred during the fast cooling from austenite temperature. Fig. 1e shows clearly some fine-grained AF in the middle of the image.

3.2. Fractographies

Fractographies of chosen CVN samples were studied using FESEM. The fractography of the original weld metal is shown in Fig. 2a, and the images of the ICHAZ-W and CGHAZ-W using the minimum and maximum cooling times (t_{8/5}) of 5 s and 30 s are presented in Fig. 2b—e. The absorbed impact toughness energy is shown as a reference in each image.

The observed fracture modes were fully ductile in original weld metal and in CGHAZ-W with $t_{8/5} = 5$ s, mostly ductile in CGHAZ-W with $t_{8/5} = 30$ s and ICHAZ-W with $t_{8/5} = 5$ s, and ductile-brittle in ICHAZ-W with $t_{8/5} = 30$ s. However, FESEM images revealed that there are local brittle regions also in original weld metal (Fig. 2a). In ICHAZ-W with $t_{8/5} = 5$ s, the brittle fracture appears to occur between ductile regions, resembling the grain boundary ferrite and ferrite side-plate regions found between AF regions in the microstructure. Grain boundary ferrite is previously reported to lower the toughness in weld metals with similar composition of the studied material (Kang et al., 2018).

Ductile fracture was characterized by the presence of dimples, which often contained small inclusions at their base. The dimples are formed due to the nucleation of microvoids around inclusions or other particles within the materials. By increasing the strain, microvoids grow, coalesce, and eventually lead to the ductile fracture (Becker and Lampman, 2002; Gladman, 1997; Pickering, 1978).

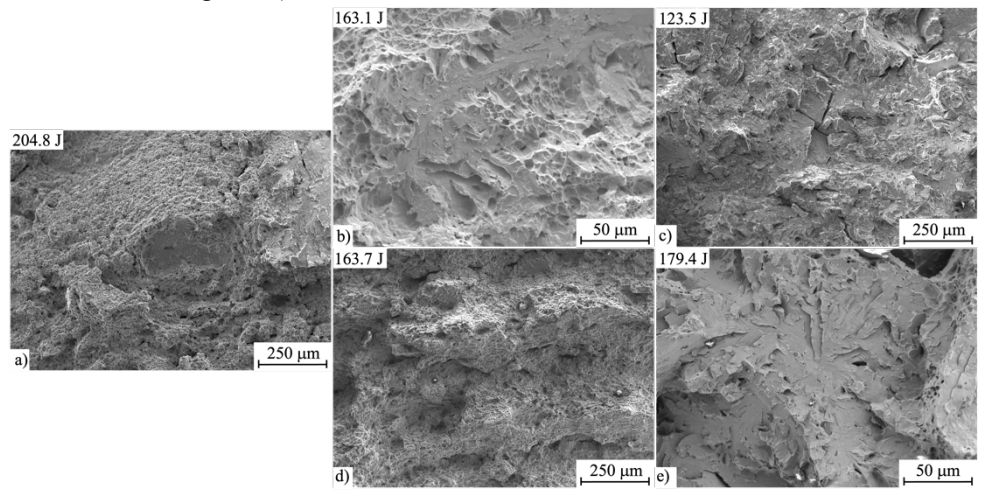


Fig. 2. Fractographies of the Charpy V-notch samples of unaffected weld metal (a), ICHAZ-W with $t_{8/5} = 5$ s (b) and 30 s (c); CGHAZ-W with $t_{8/5} = 5$ s (d) and 30 s (e).

Sharp-edged cleavage fractures were observed in ICHAZ-W with $t_{8/5} = 30$ s, which also had the lowest absorbed impact toughness energy amongst the studied samples.

Only secondary initiation sites for the brittle fracture were managed to spot in the investigated samples, whereas the primary initiation sites of the fracture were not spotted in any of the samples. Also, the brittle fracture nucleating particles were not found. This may indicate that the main concern regarding the weld metal toughness are not inclusions.

3.3. Inclusions

The primary and desired role of non-metallic inclusions in weld metals is to promote the formation of AF, which enhances the mechanical properties of the weld. To achieve this, certain types of inclusions or elements that form these inclusions are intentionally added to the weld metals. The most effective inclusions for AF formation are often small Ti- and/or Mn-bearing oxides, usually less than 3 μ m in size. However, a wide variety of inclusion types and their effect on AF formation has been previously studied (Loder et al., 2016; Sarma et al., 2009). In addition to the presence of these inclusions, other factors that promote AF formation include relatively slow cooling rates and coarse prior austenite grain size (Tervo et al., 2020).

In the present study, inclusions were analyzed in four selected samples: original weld metal, ICHAZ-W with $t_{8/5} = 5$ s, and CGHAZ-W with $t_{8/5} = 5$ s and 30 s. The scanned area was between 10–20 mm² in case of original weld and ICHAZ-W with $t_{8/5} = 5$ s. However, in CGHAZ-W with $t_{8/5} = 5$ s and 30 s, the scan was interrupted already before 4 mm² due to the detection of a large (sufficient for a comprehensive analysis) number of small inclusions, which would make the complete scan take unnecessarily long time. The size distribution of inclusions together with a cluster of small inclusions detected in CGHAZ-W is presented in Fig. 3. The size distribution shows that CGHAZ-W samples contain clearly more small inclusions than the original weld metal and ICHAZ-W. Partly this might be due to the scan settings and/or sampling effect. However, the difference is so big that likely the CGHAZ thermocycle had some effect on the inclusion content too. The majority of all inclusions in CGHAZ-W samples are very small 1–2 µm but the number density of inclusions in size groups 2–4 µm is also greater than in original weld metal and ICHAZ-W. The great number of these small inclusions may have promoted the AF formation in CGHAZ-W with $t_{8/5} = 5$ s, even if generally slower cooling would be more optimal for AF formation. In the original weld metal the number density of inclusions is generally low and interestingly there are more coarser inclusions ≈ 4 –8 µm than small ones. In ICHAZ-W no big differences to the inclusion content of the original weld were seen.

Type distribution of inclusions classified by Karakterizer, together with chemical composition map of one inclusion in the original weld metal are presented in Fig. 4. According to Karakterizer, the main inclusion types in all samples are OX,MnS and OX,MnS,TiN. However, Karakterizer is currently optimized for Al-killed and Ca-treated steel,

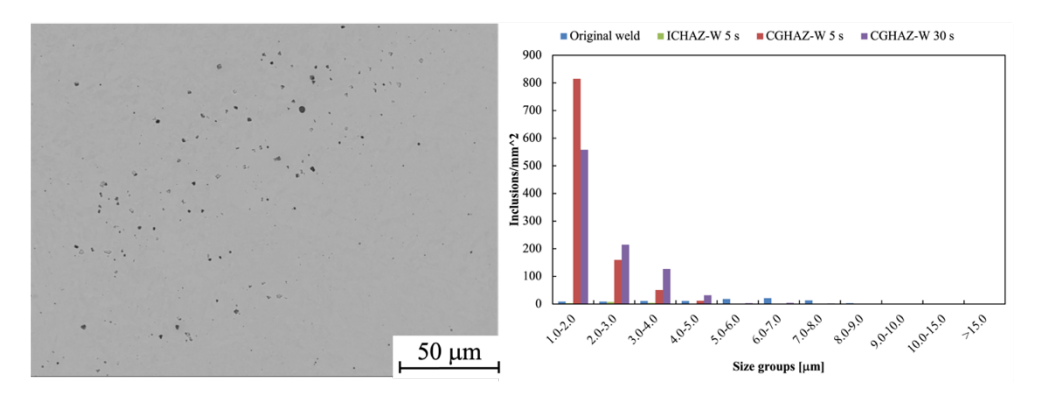


Fig. 3. Cluster of small inclusions in CGHAZ-W with $t_{8/5} = 5$ s and the size distribution of inclusions in original weld metal, ICHAZ-W with $t_{8/5} = 5$ s, CGHAZ-W with $t_{8/5} = 5$ s and CGHAZ-W with $t_{8/5} = 30$ s

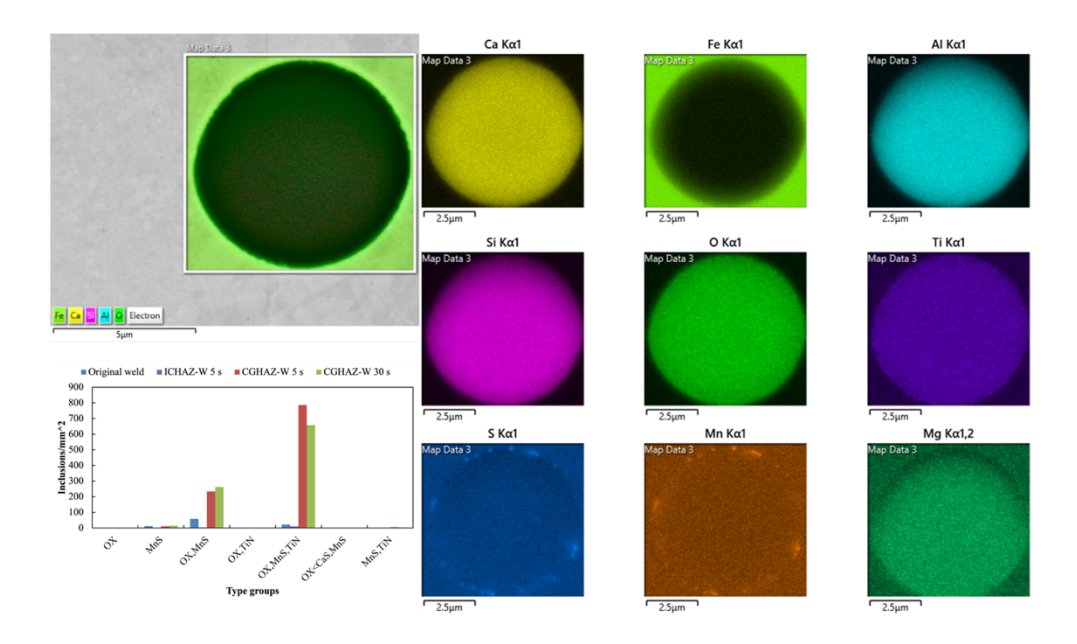


Fig. 4. Inclusion type distribution in original weld metal, ICHAZ-W with $t_{8/5} = 5$ s, CGHAZ-W with $t_{8/5} = 5$ s and CGHAZ-W with $t_{8/5} = 30$ s, and chemical composition map of one inclusion in original weld metal.

which has generally rather different inclusion content than the weld filler materials. Therefore, for example Ti is considered to appear together with nitrogen as a nitride, and the existence of titanium oxides is not considered.

EDS-maps were constructed for visualizing the actual chemical composition in a chosen inclusion from original weld metal. According to Karakterizer this inclusion belongs to the group of OX,MnS,TiN. However, the map reveals that the inclusion consists mainly of oxide of Ca, Al, Si, Ti and Mg, whereas a small amount of MnS can be found on the surface of the inclusion.

The increased number density of MnS-bearing oxides was characterized in CGHAZ-W samples. The thermocycle at the peak temperature of 1350 °C may have promoted the nucleation and growth of MnS on the surfaces of oxides. This would explain also the large number of small inclusions (1–2 μm) in CGHAZ-W samples as in original weld metal and ICHAZ-W samples the inclusions might have been below the minimum size of 1 μm and therefore were not detected. In the recent paper of Ali *et al.* (2024) the number of MnS-bearing inclusions was observed to increase in accelerated cooling of steel compared to the quenching indicating the potential of MnS to nucleate and grow in elevated temperatures (Ali et al., 2024).

MnS-bearing oxides are known to promote the formation of AF (Mabuchi et al., 1996), which supports the conclusion that the increasing number of these inclusions attributed to the fine-structured AF seen in CGHAZ-W samples (Fig. 1).

4. Conclusions

Physical simulation was performed by Gleeble 3500 thermomechanical simulator to produce HAZs on the preexisting weld metal joining two pieces of a 500 MPa offshore steel. The studied simulated HAZ regions included intercritical (ICHAZ-W) and coarse-grained HAZ of the weld (CGHAZ-W) with three different cooling times from 800 °C to 500 °C (t_{8/5}), specifically 5 s, 15 s and 30 s. The aim was to investigate the effect of the thermal cycles on the microstructures, inclusion contents and fracture surface of CVN samples on the weld metal. Following conclusions were made:

• The original weld metal mainly consisted of AF nucleated on oxide inclusions, but also grain boundary ferrite and ferrite side-plates were observed.

- A slight hardening was observed in CGHAZ-W with $t_{8/5} = 5$ s, whereas other simulated microstructures did not differ remarkably from the original weld metal when it comes to the hardness.
- Small brittle fracture regions were seen on the fractographies, even in case where the overall fracture was fully
 ductile.
- In some cases, brittle fracture regions appeared between ductile fracture regions, resembling grain boundary ferrite regions in otherwise acicular ferritic microstructures.
- A large number of small (1–4 μ m) mixed oxides were detected in CGHAZ-W with $t_{8/5} = 5$ s and 30 s, whereas in the original weld metal and ICHAZ with $t_{8/5} = 5$ s the number density of inclusions was much lower and majority of them were in the size groups of 4–8 μ m. Majority of the detected inclusions were MnS-bearing oxides.
- Increased number of small MnS-bearing oxides attributed to the fine-structured acicular ferritic microstructure in CGHAZ-W samples.

Acknowledgements

The authors are grateful to the funding of the research program FOSSA II (Fossil-Free Steel Applications, Dnro 5562/31/2023) funded by Business Finland; János Bolyai Research Scholarship of the Hungarian Academy of Sciences (Grant number: Bo/00643/22/6); Jane ja Aatos Erkon säätiö (JAES) and Tiina ja Antti Herlinin säätiö (TAHS) for their financial supports on Advanced Steels for Green Planet project.

References

Alatarvas, T., 2018. Evolution of inclusion population in calcium treated ultra-high strength steels: novel applications of sample data treatment (Dissertation). University of Oulu, Oulu.

Ali, M., Alatarvas, T., Kömi, J., 2024. Impact of niobium addition and non-metallic inclusions' characteristics on the microstructure and mechanical properties of low-carbon CrNiMnMoB ultrahigh-strength steel: A comprehensive investigation. Journal of Materials Research and Technology 30, 6133–6153. https://doi.org/10.1016/j.jmrt.2024.05.002

Becker, W.T., Lampman, S., 2002. Fracture appearance and mechanisms of deformation and fracture. Materials Park, OH: ASM International, 2002. 559–586. https://doi.org/10.1361/asmhba0003537

Gáspár, M., Kovács, J., Tervo, H., Kaijalainen, A., Javaheri, V., Sainio, J., Kömi, J., 2024. The microstructure and fracture mode of physically simulated heat-affected zones of a weld metal used with 500 MPa offshore steel – part 1: impact toughness test results. Structural Integrity Procedia. (under publication)

Gladman, T., 1997. The Physical Metallurgy of Microalloyed Steels. Maney Publishing, Leeds.

Kang, Y., Park, G., Jeong, S., Lee, C., 2018. Correlation Between Microstructure and Low-Temperature Impact Toughness of Simulated Reheated Zones in the Multi-pass Weld Metal of High-Strength Steel. Metallurgical and Materials Transactions A 49, 177–186. https://doi.org/10.1007/s11661-017-4384-3

Loder, D., Michelic, S.K., Bernhard, C., 2016. Acicular Ferrite Formation and Its Influencing Factors-A Review. Journal of Materials Science Research 6, 24. https://doi.org/10.5539/jmsr.v6n1p24

Mabuchi, H., Uemori, R., Fujioka, M., 1996. The Role of Mn Depletion in Intra-Granular Ferrite Transformation in the Heat Affected Zone of Welded Joints with Large Heat Input in Structural Steels. ISIJ International 36, 1406–1412. https://doi.org/10.2355/isijinternational.36.1406

Mičian, M., Winczek, J., Harmaniak, D., Koňár, R., Gucwa, M., Moravec, J., 2020. Physical Simulation of Individual Heat-Affected Zones in S960MC Steel. Archives of Metallurgy and Materials 66, 81–89. https://doi.org/10.24425/amm.2021.134762

Pickering, F.B., 1978. Physical metallurgy and the design of steels. Applied Science Publishers Ltd., London.

Sarma, D.S., Karasev, A. V, Jönsson, P.G., 2009. On the Role of Non-metallic Inclusions in the Nucleation of Acicular Ferrite in Steels. ISIJ International 49, 1063–1074. https://doi.org/10.2355/isijinternational.49.1063

Tervo, H., Kaijalainen, A., Javaheri, V., Kolli, S., Alatarvas, T., Anttila, S., Kömi, J., 2020. Characterization of coarse-grained heat-affected zones in al and ti-deoxidized offshore steels. Metals (Basel) 10, 1–18. https://doi.org/10.3390/met10081096

Tervo, H., Seppälä, O., Alatarvas, T., Hannula, J., Pallaspuro, S., Kömi, J.I., 2023. A Study on Inclusion Characterisation of Steel Using a Novel Inclusion Characterisation Tool. Key Eng Mater 968, 39–44. https://doi.org/10.4028/p-ti9cwa

Tezuka, N., Shiga, C., Yamaguchi, T., Bosansky, J., Yasuda, K., Kataoka, Y., 1995. Toughness Degradation Mechanism for Reheated Mo-Ti-B Bearing Weld Metal. ISIJ International 35, 1232–1238. https://doi.org/10.2355/isijinternational.35.1232

Węglowski, M.S., Zeman, M., Lomozik, M., 2013. Physical Simulation of Weldability of Weldox 1300 Steel. Materials Science Forum 762, 551–555. https://doi.org/10.4028/www.scientific.net/MSF.762.551

Willms, R., 2009. High strength steel for steel constructions. Nordic Steel Construction Conference. Malmö, Sweden 597-604.

Xiong, Z., Liu, S., Wang, X., Shang, C., Li, X., Misra, R.D.K., 2015. The contribution of intragranular acicular ferrite microstructural constituent on impact toughness and impeding crack initiation and propagation in the heat-affected zone (HAZ) of low-carbon steels. Materials Science and Engineering: A 636, 117–123. https://doi.org/10.1016/j.msea.2015.03.090